Available online at www.sciencedirect.com
ScienceDirect
Trans. Nonferrous Met. Soc. China 30(2020) 548−558
Transactions of Nonferrous Metals Society of China
www.tnmsc.cn

Electrodeposition and corrosion behavior of Zn−Ni−Mn alloy coatings deposited from alkaline solution

Babak ABEDINI[1], Naghi PARVINI AHMADI[1], Sasan YAZDANI[1], Luca MAGAGNIN[2]

1. Faculty of Materials Engineering, Sahand University of Technology, Tabriz, Iran;
2. Dipartimento di Chimica, Materiali e Ingegneria Chimica Giulio Natta, Politecnico di Milano, Via Mancinelli 7, 20131, Milano, Italy

Received 15 December 2018; accepted 25 November 2019

Abstract: The potentiostatic electrodeposition of Zn−Ni−Mn was carried out in an alkaline solution with the addition of Mn salt. The effects of electrolyte Mn^{2+} concentration and deposition potential on the surface morphology, phase structure and corrosion behavior of coatings were studied. The results of corrosion polarization showed that the presence of higher Mn content in Zn−Ni−Mn coatings could lead to the formation of a good passive layer with a 7-fold increase in R_p of coating and a significant decrease in the corrosion current density compared to those of Zn−Ni coating. The XRD and the XPS analyses from the surface of Zn−Ni−Mn after corrosion test showed that the passive layer was composed of zinc hydroxide chloride, zinc oxide, zinc hydroxide carbonate, and manganese oxides.
Key words: Zn−Ni−Mn; electrodeposition; alkaline bath; phase structure; corrosion resistance; chemical composition

1 Introduction

Zinc-based coatings have been found many applications in industry as sacrificial anodes to protect steel components. The high dissolution rate of pure zinc in corrosive media is the main drawback of these coatings [1−3]. In order to overcome this problem, various alloying elements have been added to improve the corrosion resistance of Zn. The incorporation of alloying elements such as Fe, Co and Ni in the structure of zinc coatings shifts the corrosion potential to nobler values and also reduces the corrosion current density. Among these alloys, Zn−Ni, due to its good corrosion and mechanical properties, has attracted great attention in recent years as a potential substitute for Cd [4−10]. Zn−Ni coatings provide better corrosion protection than zinc, and the corrosion mechanism consists of sacrificial dissolution of zinc in the corrosive media and formation of low soluble corrosion products on the surface of the coating. Zn−Ni coatings deposited in alkaline baths show better quality of element distribution and morphological uniformity compared with those deposited in acidic electrolytes [11,12]. Zn−Ni coatings with 12−15 wt.% Ni show the highest corrosion protection while in coatings with higher Ni content, the sacrificial properties of deposits are decreased [13]. Furthermore, according to various literatures, the addition of a third alloying element such as Cd, Fe, Co and P or a ceramic reinforcement such as Al_2O_3 and carbon nano-tube can effectively improve the corrosion resistance of the Zn−Ni deposits [9,14−20].

Zn−Mn alloy coatings are also known to show high corrosion protection. The equilibrium potential of $Mn/Mn^{2+}$is less noble than that of Zn/Zn^{2+} and Ni/Ni^{2+}. Thus, the protection mechanism in this alloy is different from other Zn alloy coatings. The double-protection mechanism proposed by

Corresponding author: Naghi PARVINI AHMADI; E-mail: parvini@sut.ac.ir
DOI: 10.1016/S1003-6326(20)65234-7

BOSHKOV et al [21] begins with the sacrificial dissolution of less noble Mn in the corrosive media and the subsequent increase in pH of the solution at the surface of the coatings [22]. This enhances the formation of a compact and thick protective layer [23]. Moreover, the addition of Mn as a third alloying element to Zn−Ni and Zn−Mo coatings significantly enhances the corrosion protection of these coatings by the formation of a more corrosion resistant passive layer [24,25]. The successful electrodeposition of Zn−Ni−Mn coatings from acidic sulfate and sulfate−citrate electrolytes has been reported [25−27]. The electrodeposition of this alloy coating in alkaline electrolytes has not been reported in the literature to the best of our knowledge.

The purpose of this work was to study the feasibility of Mn co-deposition with Zn and Ni from an alkaline Zn−Ni electrolyte, and to investigate the effect of various amounts of Mn on the corrosion protection of Zn−Ni−Mn coatings. The effect of adding various amounts of Mn additive to Zn−Ni deposition electrolytes on the electrodeposition behavior was investigated by cyclic and linear sweep voltammetry techniques. Zn−Ni−Mn alloy coatings were deposited potentiostatically. Scanning electron microscopy (SEM) was used to investigate the surface morphology of samples. Energy dispersive spectroscopy (EDS) and X-ray fluorescence (XRF) were used to identify the changes in the chemical composition of coatings. XRF was also used to measure the thickness of coatings. X-ray diffraction (XRD) was used to characterize the phase structure and crystallite size of the coatings. Moreover, anodic polarization was used to study the effect of addition of various amounts of Mn on the corrosion behavior of coatings in NaCl solution. X-ray photoelectron spectroscopy (XPS) and XRD were used to determine the chemical composition of the corrosion products formed on the surface of Zn−Ni and Zn−Ni−Mn samples after corrosion tests.

2 Experimental

2.1 Preparation of electrodeposition solution

The Zn−Ni alkaline electrodeposition solution composed of NaOH, ZnO, ethylenediamine (ED), triethanolamine (TEA) and Ni additive (5 vol.% ED, 10 vol.% TEA, and 360 g/L $NiSO_4$) was used as a base solution. In order to investigate the effect of Mn addition, $MnSO_4$ was added to the base solution. The addition of $MnSO_4$ to the transparent base solution (in the absence of Ni additive) changed the color to pink due to the formation of manganese hydroxide particles. Subsequently, white manganese oxide precipitates were formed at the bottom of the glass container. In order to avoid this reaction, Mn was complexed with sodium gluconate in another container and the resulting solution was added to the base solution as Mn additive. The choice of sodium gluconate as an additive was made because it has been successfully used as Mn- complexing agent in the high pH range [28]. A solution of Mn additive was made by dissolving 0.53 mol/L $MnSO_4$ and 0.64 mol/L sodium gluconate in deionized water. In order to elucidate the effect of Mn concentration on the deposition of Zn−Ni−Mn alloy coatings, 100 mL Zn−Ni electroplating solution with various Mn^{2+} concentrations (0.57, 1.14, 1.71 and 2.28 μmol/L) was prepared. However, adding more than 2.28 μmol/L Mn^{2+} to the base solution led to the formation of dark brown Mn oxide particles in the solution. The continuous variation in color of the solutions, containing different amounts of Mn, from red to dark brown with time corresponds to the change in the oxidation state of Mn complexes in NaOH solution. Thus, Zn−Ni−Mn solutions were left unstirred for 5 h in order for them to stabilize prior to electrodeposition. A sample coding pattern on the basis of the concentration of Mn^{2+} in the electrolyte and electrodeposition potential used in this work is given in Table 1 (e.g., sample A-1 means the sample electrodeposited in 0.19 μmol/L Mn^{2+} containing electrolyte (bath A) at −1780 mV (vs Ag/AgCl) potential).

Table 1 Sample coding system based on Mn^{2+} concentration in electrolyte and electrodeposition potential

Code	Mn^{2+} concentration/ ($\mu mol \cdot L^{-1}$)	Code	Electrodepositon potential (vs Ag/AgCl)/mV
A	0.19	1	−1780
B	0.57	2	−1820
C	1.14	3	−1860
D	1.71	4	−1900
E	2.28	5	−1940

2.2 Electrochemical analyses

All the electrochemical measurements were carried out using Amel 2551 Potentiostat/ Galvanostat and a saturated Ag/AgCl electrode as a reference electrode. Pt wire was used as the counter electrode in cyclic voltammetry, linear sweep voltammetry, and corrosion measurements, whereas Ni mesh was used as the counter electrode in electrodeposition. In order to study the electrochemical reactions involved in Zn−Ni−Mn alloy deposition, cyclic voltammetry (CV) was carried out on a glassy carbon electrode as the working electrode in a solution containing 1.71 μmol/L Mn^{2+}. The potential sweep was from 0 to −2 V at a scan rate of 10 mV/s. Cathodic linear sweep voltammetry of steel samples with 0.01 mV/s scan rate was employed to study the effect of various concentrations of Mn additive on the electrochemical behavior of alloy deposition. Prior to electrodeposition, 1.5 cm × 2 cm mild steel sheets were polished with emery paper to 1200 grit and sonicated in acetone for 10 min. Then, all samples were etched in 35% HCl and rinsed in deionized water. The Zn−Ni−Mn alloy coating was electrodeposited potentiostatically on 1.5 cm^2 exposed area of the substrate and the remaining area was masked by Kapton tape. In order to study the corrosion behavior of coatings, anodic polarization measurements were performed in aerated 3.5 wt.% NaCl solution at the room temperature. Samples with 1 cm^2 in exposed surface area and 12 μm in thickness were used for corrosion analysis. All samples were stabilized in the NaCl solution for 30 min prior to each measurement. The potential sweep was carried out at ±500 mV of open circuit potential (φ_{OCP}) with 1 mV/s.

2.3 Coating characterization

Zeiss EVO 50 EP scanning electron microscopy (SEM) was used to observe the effects of Mn concentration and electrodeposition potential on the surface morphology of coatings. Energy dispersive spectroscopy (EDS, Oxford Instrument, INCA Energy 200) and X-ray fluorescence (XRF, Fischerscope X-ray XAN) measurements were used to determine the chemical composition of coatings. The thickness of coatings was also measured by XRF. The phase structure of coatings was characterized by X-ray diffraction (XRD, Philips-PW 1830) using Cu K_α radiation (λ=1.5405 Å). A method suggested by Wilson and Rogers was applied to determining the preferred orientation of electrodeposited coatings, and the Williamson−Hall method was used to measure the crystallite size of coatings. The crystallite size was estimated according to the modified Scherrer formula:

$$B_{hkl}\cdot\cos\theta=0.9\lambda/D+C\cdot\varepsilon\cdot\sin\theta \quad (1)$$

where B_{hkl} is the full width at the half maximum of the XRD peaks, D is the crystallite size, θ is the Bragg angle, and ε is the lattice strain. The crystallite size was extracted from the intercept of Williamson−Hall plot ($B_{hkl}\cdot\cos\theta$ vs $C\cdot\sin\theta$ plot) [29,30].

The chemical composition of the surface of Zn−Ni and Zn−Ni−Mn alloy coatings after corrosion test was determined via the XRD and the X-ray photoelectron spectroscopy (XPS, SPECS PHOIBOS 150 analyzer). The XPS spectra were obtained using K_α radiation (1486.6 eV).

Moreover, in order to study the protective properties of the coatings, neutral salt spray test was carried out according to ASTM B 117, using 5 wt.% NaCl solution.

3 Results and discussion

A solution with a high concentration of Mn^{2+} was chosen for cyclic voltammetry. Figure 1 shows the CV of a glassy carbon electrode in a bath containing 1.71 μmol/L Mn^{2+}. In the negative scan, two current peaks are evident; the first one c_1 at −0.46 V (vs Ag/AgCl) can be attributed to Ni^{2+} reduction which is close to Ni/Ni^{2+} equilibrium potential, and the second one c_2 at −1.62 V corresponds to Zn^{2+} reduction. The parasitic reaction of hydrogen evolution occurs simultaneously with Zn reduction and drastically increases the cathodic current density. This also masks peaks related to the reduction of Mn ions. Afterwards, a crossover loop is observed in the positive direction scan suggesting a nucleation process. Several oxidation peaks are observed during the positive scan, from −1.3 to −0.6 V, corresponding to the dissolution of metals from different phases in the coating. Peaks a_1 and a_2 at potentials of −1.25 and −1.03 V can be related to Zn dissolution from η and γ phases of Zn−Ni, while anodic peak a_3 represents the dissolution of Ni from the coating [11,31,32].

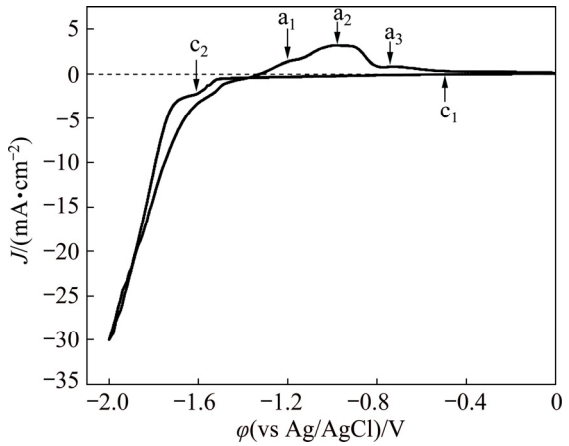

Fig. 1 Cyclic voltammogram of glassy carbon electrode in bath containing 1.71 μmol/L Mn^{2+} (scan rate 10 mV/s)

The effect of Mn additive concentration on linear sweep voltammetry of steel electrode is illustrated in Fig. 2. Due to steel corrosion at more positive potentials, voltammetry was carried out from −0.9 to −2 V. Compared to glassy carbon electrode, Zn^{2+} reduction occurs at more positive potential. This can be attributed to higher over-potential of Zn deposition on the surface of the glassy carbon. It is obvious from Fig. 2 that adding the higher concentration of Mn to the solution reduces the cathodic current density in potentials more negative than −1.8 V.

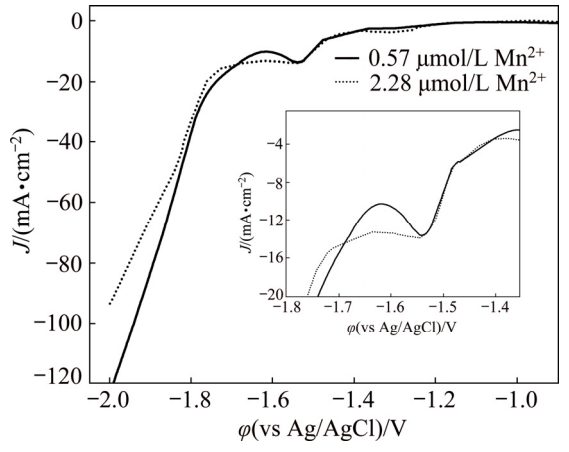

Fig. 2 Effect of Mn ion concentration in electrolyte on linear sweep voltammogram of medium steel electrode (scan rate 0.01 mV/s)

The electrodeposition potential range from −1780 to −1940 mV (vs Ag/AgCl) was chosen based on cyclic voltammetry results in order to study the effect of potential on microstructure, chemical composition and phase structure of the coatings. In order to ensure the presence of a high concentration of Mn ions, a bath containing 2.28 μmol/L Mn^{2+} was used. Initially, some test samples were deposited in more positive potentials (from −1570 to −1740 mV), but XRF did not show any amount of Mn in the coatings deposited in this particular potential range.

It is clear from the XRF results (Fig. 3(a)) that by increasing the potential to more negative values in solutions containing 2.28 μmol/L Mn^{2+} ions, the Mn content of coatings increased significantly from 2.72 wt.% at −1780 mV to 11.6 wt.% at −1940 mV while Ni content decreased from 13.8 to 7.7 wt.%. A similar trend can be seen for increasing the Mn^{2+} ions concentration in the electrolyte from 0.19 to 2.28 μmol/L (Fig. 3(b)). A-3 sample was composed of less than 1 wt.% Mn and 15.9 wt.% Ni, and E-3 was composed of 9.69 wt.% Mn and 9.41 wt.% Ni. However, the highest Mn content was achieved in E-5 sample (11.6 wt.% Mn and 7.7 wt.% Ni).

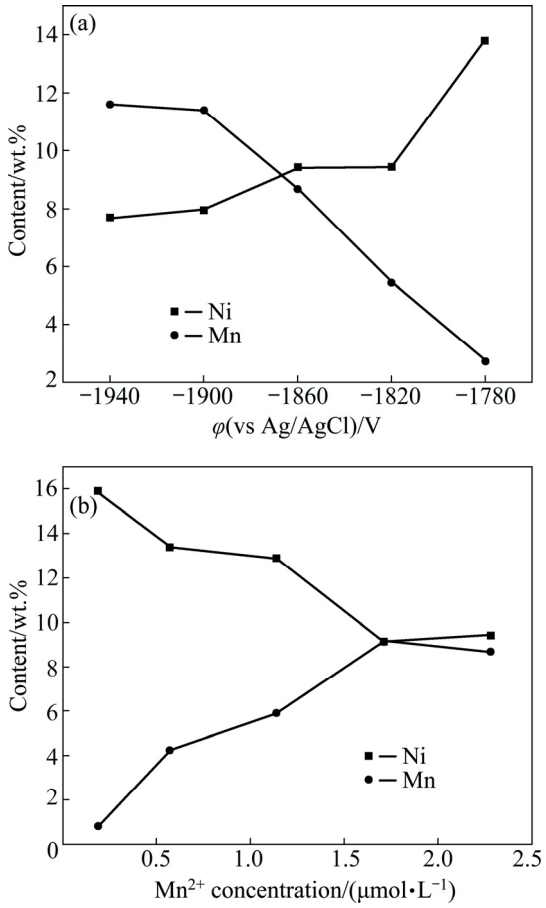

Fig. 3 Ni and Mn contents of coatings electrodeposited in 2.28 μmol/L Mn^{2+} electrolyte at various potentials (a) and coatings electrodeposited at −1860 mV in electrolytes containing various concentrations of Mn^{2+} (b)

The influence of electrolyte composition and electrodeposition potential on the surface morphology of coatings is shown in Fig. 4. Increasing the Mn concentration significantly affects the surface morphology. In Fig. 4(a), various non-closed U-shaped morphologies ranging from 25 to 45 μm on the surface of C-3 coating can be seen. These are surrounded by a large quantity of smaller globular nodules randomly formed on the surface of the coating. The surfaces of D-3 and E-3 coatings (Figs. 4(c, e)) are smoother and no sign of U-shaped morphologies can be seen. Also, the number of globular nodules on the surface of these samples decreased significantly.

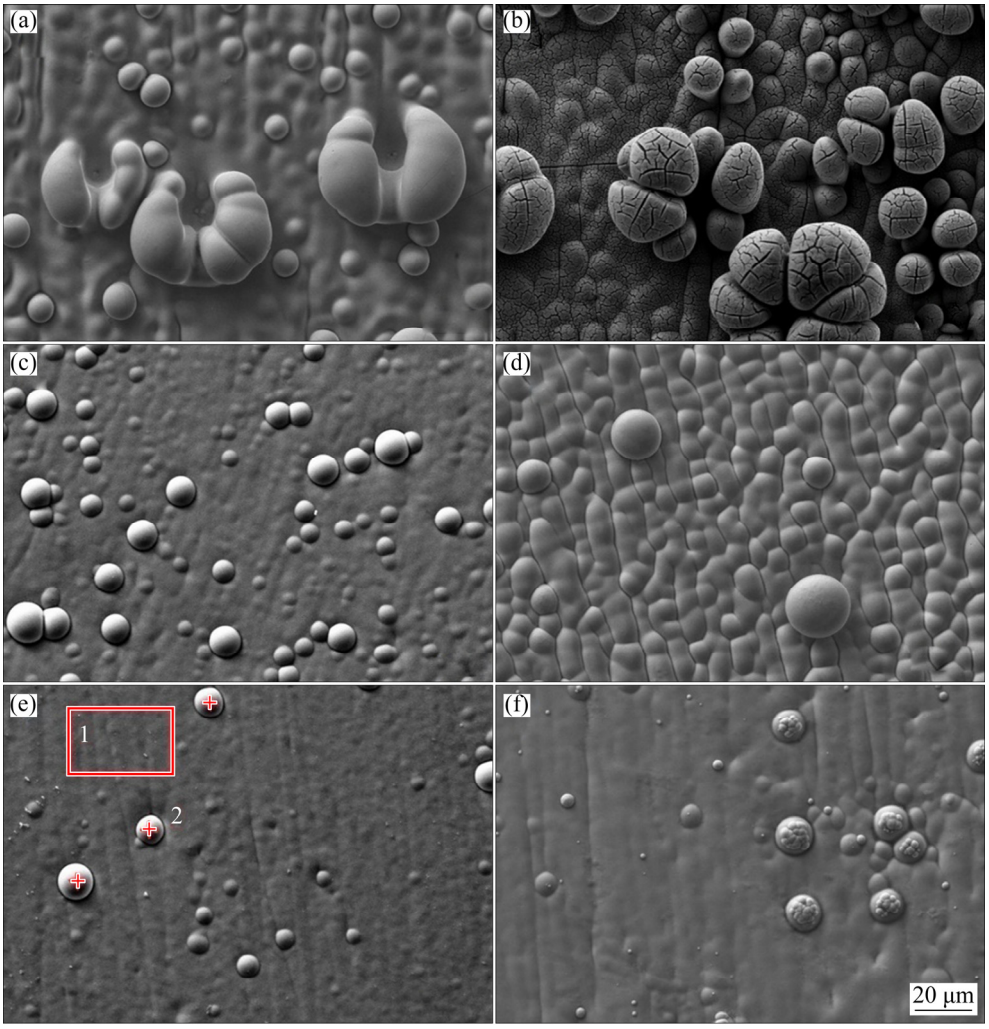

Position	Content/wt.%			
	Mn	Ni	Zn	Total
Underlying film	11.66	9.06	79.28	100.00
Surface nodules	10.88	10.26	78.86	100.00
Low magnification	11.02	8.56	80.45	100.00

Fig. 4 SEM micrographs of coatings deposited in 1.14 μmol/L (a, b), 1.71 μmol/L (c, d) and 2.28 μmol/L (e, f) Mn^{2+} electrolyte, at electrodeposition potentials of −1860 mV (a, c, e) and −1940 mV (b, d, f) (vs Ag/AgCl), and chemical composition of underlying layer and average of three nodules, and low magnification EDS spectrum of E-3 sample (g)

The EDS analysis from the surface of E-3 sample shows a small difference between the chemical composition of underlying film and surface nodules (Fig. 4(g)). Similar to this sample, the Ni and Mn contents of globular nodules in the other coatings are lower than those in the underlying surface. The presence of some pin holes on the surface of these coatings is due to hydrogen evolution. It is obvious from the SEM micrograph that an increase in electrodeposition potential from −1860 to −1940 mV, increases the grain size of the coatings. The average size of nodules on the surface of D-3 (Fig. 4(c)) is about 7 μm, while it increases to 20 μm in D-5 sample (Fig. 4(d)). The SEM micrographs with higher magnification show that C-5 consists of many fine micro-cracks both at the surface and in the nodules (Fig. 4(b)).

Considering the binary phase diagrams of Zn−Ni and Zn−Mn, various phases could be formed in Zn−Ni−Mn alloy coatings. Zn−Mn coatings are mostly composed of a solid solution of Mn in Zn with Mn content less than 1 at.%, and intermetallic phases ζ and ε. According to Zn−Mn phase diagram, ζ ($ZnMn_{13}$) is obtained when the Mn content is lower than 10.2 at.%, while ε phase usually appears above 200 °C with the Mn content being between 11 and 58 at.% [33].

However, the presence of the ε phase in the coatings with a lower amount of Mn at room temperature has also been reported [34]. On the other hand, Zn−Ni alloy coatings with Ni content less than 15 wt.% consist of η phase, a solid solution of Ni in Zn, and γ (Ni_5Zn_{21}), an intermetallic phase [31].

The XRD patterns of samples electrodeposited at −1860 mV (vs Ag/AgCl) in Zn−Ni−Mn electrolyte with different concentrations of Mn additive are reported in Fig. 5(a). The chemical composition of coatings was largely dependent on the Mn concentration in electro-deposition baths. It has been shown in Fig. 3 that by increasing the amount of Mn additive, the Mn content of coatings increased from 0.82 wt.% in A-3 sample to 9.69 wt.% in D-3 sample, while the Ni content decreased from 15.1 wt.% to 9.41 wt.% in A-3 and D-3 samples, respectively.

The diffractogram of A-3 sample corresponds to a two-phase Zn−Ni structure, composed of η and γ phases. As it can be seen, the diffractograms of other samples resemble that of A-3 sample and the difference is in the slight shift towards a lower angle in the position of the peaks and a lower intensity (Table 2). This indicates that Mn is incorporated in the lattice of Zn−Ni phases (Fig. 5(a)).

The influence of electrodeposition potential on

Table 2 Effect of Mn^{2+} concentration in electrolyte on shift of γ phase XRD peaks position electrodeposited at −1860 mV (vs Ag/Ag/AgCl) shown in Fig. 5(a)

Mn^{2+} concentration/ (μmol·L^{-1})	2θ/(°)			
0.19	42.928	62.382	78.531	89.183
0.57	42.840	61.963	78.220	88.641
1.14	42.616	61.921	77.848	88.591
1.71	42.543	61.691	77.637	88.063
2.28	42.538	61.529	77.620	88.020

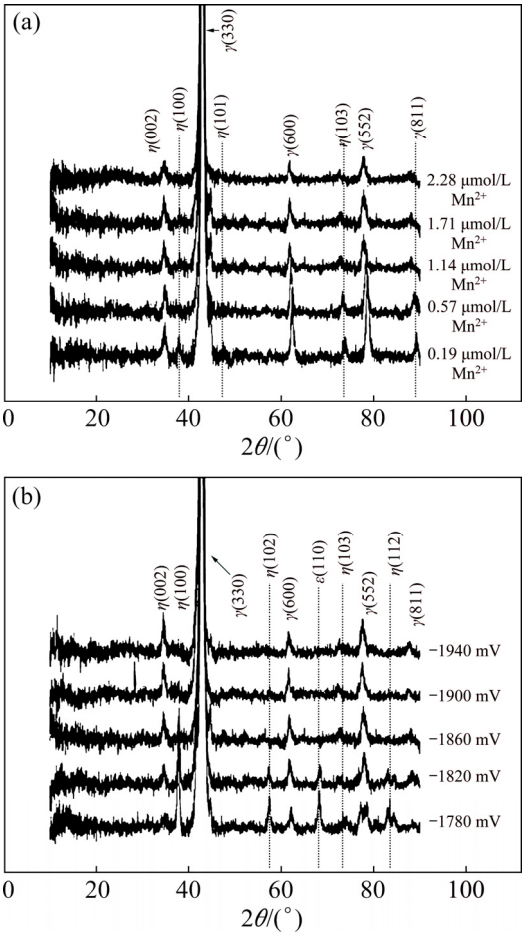

Fig. 5 XRD patterns of coatings deposited at −1860 mV (vs Ag/AgCl) from electrolytes containing different concentrations of Mn^{2+} (a) and deposited from 2.28 μmol/L Mn^{2+} electrolyte at various potentials (b)

the phase structure of coatings deposited in 2.28 μmol/L Mn^{2+}-containing electrolyte is shown in Fig. 5(b). The XRD patterns of coatings deposited at more positive potentials such as −1780 and −1820 mV reveal the presence of peaks corresponding to ε phase (2θ=68.3°) in addition to those of η and γ phases. As previously mentioned, ε phase was observed in deposits with Mn content higher than 10.2 at.%; however, Fig. 3 shows that the Mn content of E-1 and E-2 samples (2.28 μmol/L Mn^{2+}, −1780 and −1820 mV) is lower than this value.

It is interesting to note that the ε phase peaks disappeared by increasing the electrodeposition potential despite the increase in the Mn content of coatings up to 12 wt.%.

The increase of Mn content of coatings by increasing the potential and additive concentration in the bath did not affect the preferred orientation of crystallites. In all samples, (330) has the highest orientation index and the preferred orientation.

The crystallite size variation with deposition potential in samples electrodeposited in 2.28 μmol/L Mn^{2+} electrolyte (bath E) is shown in Fig. 6. By increasing the electrodeposition potential, the crystallite size decreases from 28 nm at −1780 mV (vs Ag/ AgCl) to 16 nm at −1940 mV. An increase in electrodeposition potential increases the nucleation rate and consequently decreases the crystallite size.

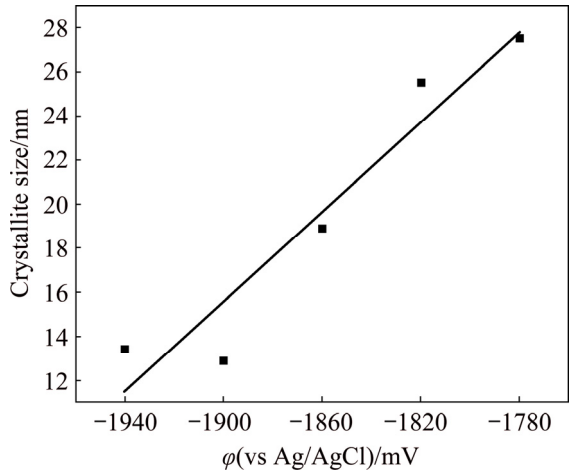

Fig. 6 Effect of deposition potential on crystallite size of coatings deposited from 2.28 μmol/L Mn^{2+} solution

The polarization curves of Zn−Ni−Mn coatings electrodeposited at −1860 mV in the electrolytes with various concentrations of Mn^{2+} are shown in Fig. 7. The corrosion current density (J_{corr}) and corrosion potential (φ_{corr}) were determined using Tafel extrapolation. Adding Ni to Zn coatings shifts the φ_{corr} to nobler potentials, while Mn due to its less noble nature shifts the φ_{corr} of Zn−Ni coatings to more negative potentials. An increase in the Mn^{2+} concentration of Zn−Ni−Mn coatings is accompanied by a reduction in Ni concentration (Fig. 3). Thus, the decrease in the corrosion potentials shown in Table 3 is due to the higher concentration of more electronegative Mn in the coatings.

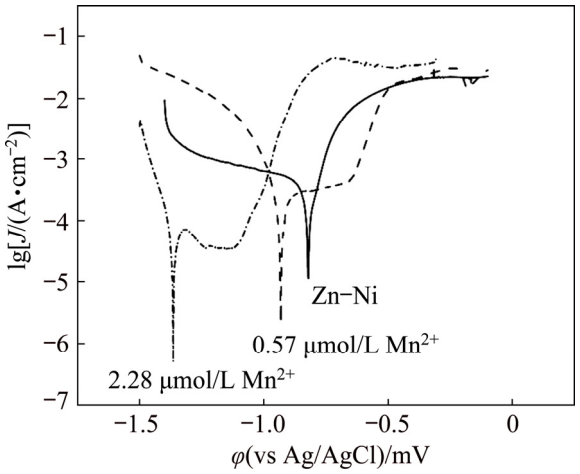

Fig. 7 Polarization curves of coatings deposited at −1860 mV (vs Ag/AgCl) with solutions containing various concentrations of Mn^{2+}

Table 3 Corrosion parameters of Zn−Ni coating and Zn−Ni−Mn alloy coatings electrodeposited at −1860 mV (vs Ag/AgCl) in solutions containing 0.57 and 2.28 μmol/L Mn^{2+}

Sample	Corrosion parameter		
	J_{corr}/(μA·cm^{-2})	φ_{corr} (vs Ag/AgCl)/mV	R_p/Ω
Zn−Ni	457	−848	138
B-3	267	−886	242
E-3	30.65	−1358	1065

A passivation behavior cannot be observed in the polarization curves of Zn−Ni coatings. The incorporation of Mn into the Zn−Ni coatings, however, changed the corrosion behavior of the coatings. The polarization curves of samples with various concentrations of Mn^{2+} are composed of a passivation region. The J_{corr} is decreased from 457 μA/cm^2 in Zn−Ni to its lowest value of 30.65 μA/cm^2 in E-3 sample. The polarization

resistance of the coatings increased from 138 Ω in Zn−Ni sample to 1065 Ω in E-3 sample, which also corresponds to the formation of a passive layer at the surface resulting in a coating with a higher protective property.

White rust formation was first observed at the surface of Zn−Ni after 96 h of exposure in the neutral salt spray chamber. While the formation of white rust on the surface of Zn−Ni−Mn coatings took longer time. It was first observed at the surface of B-3 sample with lower Mn^{2+} concentration at 144 h and then at the surface of E-3 sample in 168 h. Red rust was observed at the surface of Zn−Ni after 288 h. While first signs of formation of brown corrosion products on the surface of Mn-containing sample were observed after 408 h and no red rust was observed. This could be due to the presence of Mn compounds in the corrosion products of these coatings. It can be said that incorporation of Mn to Zn−Ni coatings significantly improved the corrosion resistance of Zn−Ni−Mn coatings.

The XRD patterns of Zn−Ni and Zn−Ni−Mn (E-3) alloy coatings, after corrosion tests, are presented in Fig. 8. The most of observed peaks, in both samples, correspond to simonkolleite ($Zn_5(OH)_8Cl_2·H_2O$) except the peak with the highest intensity, which is positioned at 2θ=42.7°, and the peaks at 2θ=28.2°, 45.5°, 62° which are associated with the presence of $NiZn_3$. The formation of $NiZn_3$ can be addressed to dezincification and migration of Zn ions from the underlying layer to the corrosion film.

The C 1s spectra of both samples are shown in Fig. 9(a). The peak is de-convoluted into three components. Two peaks at 284.4 and 286.3 eV that correspond to the organic contamination, and the third at 288.8 eV can be attributed to the presence of carbonate groups on the top layer of the surface. The O 1s spectrum of the binary alloy is composed of peaks at 530.7, 532.2, and 533.7 eV that are related to zinc oxide, simonkolleite, and hydrozincite ($Zn_5(CO_3)_2(OH)_6$), respectively (Fig. 9(b)). Hydrozincite is the product of the reaction between Zn ions and dissolved carbonate in the atmosphere [35]. The asymmetry in peak shape of O 1s toward lower binding energies in ternary alloy could be caused by the higher ratio of metal oxide compared to the binary alloy that could be due to the formation of Mn oxides. This can be confirmed by a low-intensity Mn $2p_{3/2}$ peak at 642 eV in the spectrum of ternary alloy, as shown in Fig. 9(c). It is suggested that the formation of manganese oxide hinders the reduction of oxygen on the cathode surface and subsequently decreases the corrosion rate [36].

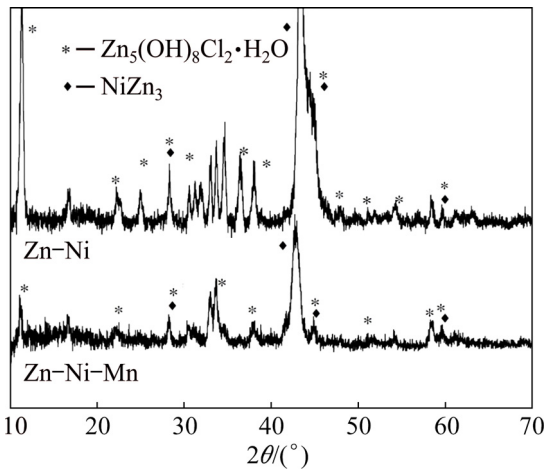

Fig. 8 XRD patterns of Zn−Ni and Zn−Ni−Mn (E-3) coatings after corrosion test

Ni 2p peaks can be observed in the XPS of the binary alloy (Fig. 9(d)), while no Ni peaks were discernible on the XPS spectrum of the ternary alloy. This can be due to the larger thickness of corrosion film in the ternary alloy. Ni $2p_{3/2}$ peak at 855.4 eV and doublet separation of 17.8 eV are characteristic of $Ni(OH)_2$.

The chemical shift between Zn 2p peaks of various chemical states of Zn is quite short, therefore it is hard to differentiate between them (Fig. 9(e)). Both the XPS and XRD were used as surface analysis methods. While the depth of sampling in XPS is limited to 3−10 nm from the surface, this is in micro-metric scale in XRD. Therefore, considering the results of the XRD and XPS methods, it can be concluded that the passive film formed on both samples is mainly composed of simonkolleite and two other zinc compounds, namely hydrozincite and zinc oxide. In addition to these compounds, the presence of $Ni(OH)_2$ on the surface of Zn−Ni coating explains the lower protective properties of this coating compared to Zn−Ni−Mn coating with Mn oxides on the surface. This also points to the reason behind the 7-fold increase in the R_p and the significant decrease of J_{corr} in Zn−Ni−Mn coating (E-3) in comparison with Zn−Ni.

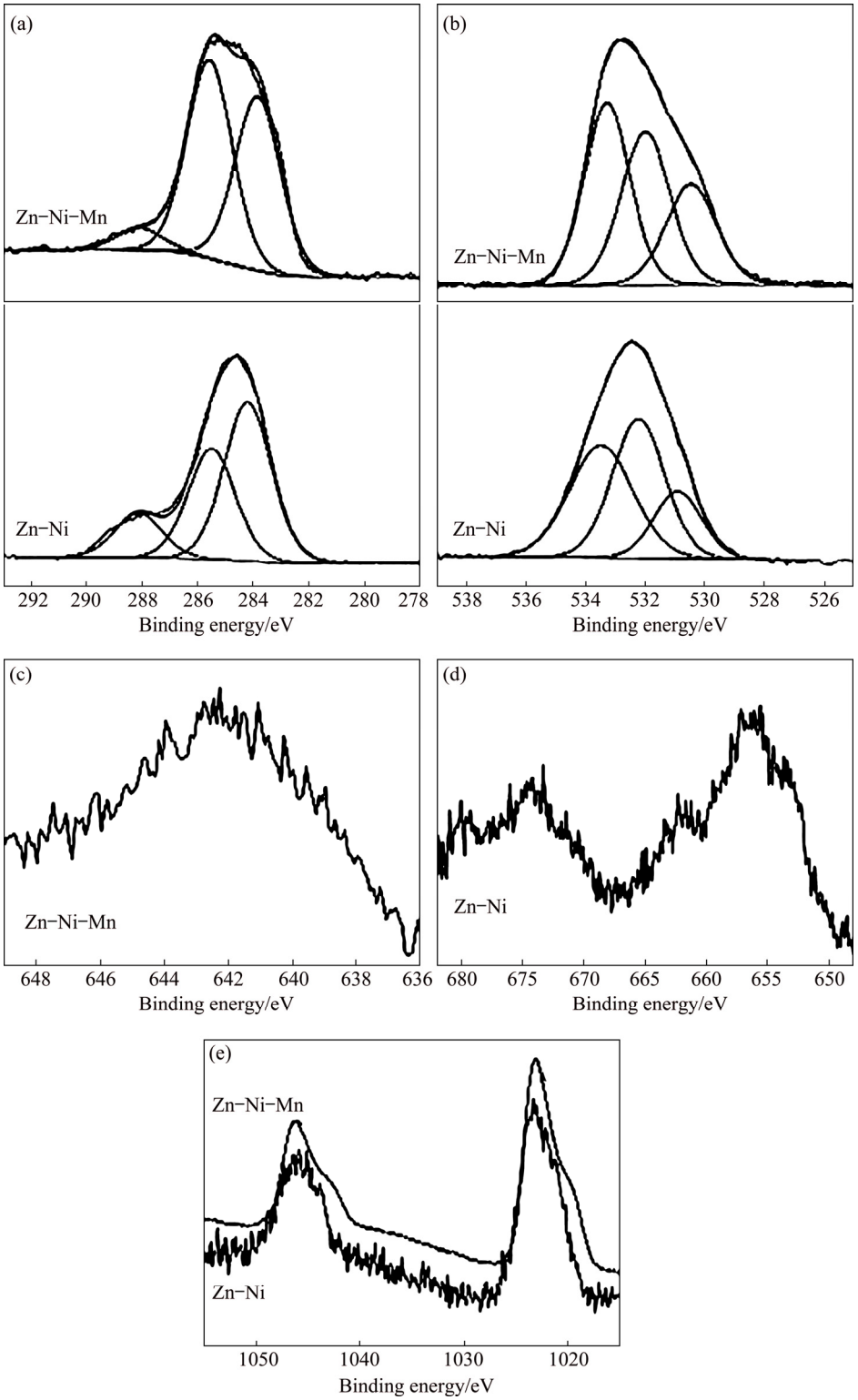

Fig. 9 C 1s (a), O 1s (b), Mn $2p_{3/2}$ (c), Ni 2p (d) and Zn 2p (e) photoelectron spectra of Zn−Ni and Zn−Ni−Mn (E-3) coatings after corrosion test

4 Conclusions

(1) Increasing both the Mn concentration of the Zn−Ni−Mn electrolyte and increasing the deposition potential increased the Mn content of the coatings, and affected the surface morphology and the phase structure of these coatings.

(2) The results of corrosion polarization showed that the presence of higher Mn content in

Zn−Ni−Mn coatings could lead to the formation of a good passive layer with a 7-fold increase in R_p of coatings.

(3) XPS and XRD analyses of the corrosion products formed at the surface of Zn−Ni and Zn−Ni−Mn (E-3) coatings showed that zinc hydroxide chloride was the main constituent in both samples. However, the layer formed at the surface of Mn-containing coating was also composed of Mn oxides that can improve the protective properties of this coating.

References

[1] CROTTY D. Zinc alloy plating for the automotive industry [J]. Metal Finishing, 1996, 94(9): 54−58. doi: 10.1016/0026-0576(96)82103-9.

[2] WILCOX G D, GABE D R. Electrodeposited zinc alloy coatings [J]. Corrosion Science, 1993, 35(5−8): 1251−1258. doi: 10.1016/0010-938X (93)90345-H.

[3] YUAN Liang, DING Zhi-ying, LIU Shi-jun, SHU Wei-fa, HE Ya-ning. Effects of additives on zinc electrodeposition from alkaline zincate solution [J]. Transactions of Nonferrous Metals Society of China, 2017, 27(7): 1656−1664. doi: 10.1016/S1003-6326(17) 60188-2.

[4] RAMANAUSKAS R, JUŠKĖNAS R, KALINIČENKO A, GARFIAS-MESIAS L F. Microstructure and corrosion resistance of electrodeposited zinc alloy coatings [J]. Journal of Solid State Electrochemistry, 2004, 8(6): 416−421. doi: 10.1007/s10008-003-0444-2.

[5] RAMANAUSKAS R, QUINTANA P, MALDONADO L, PORN R. Corrosion resistance and microstructure of electrodeposited Zn and Zn alloy coatings [J]. Surface and Coatings Technology, 1997, 92(1−2): 16−21. doi: 10.1016/S0257-8972(96)03125-8.

[6] TAFRESHI M, ALLAHKARAM S R, FARHANGI H. Comparative study on structure, corrosion properties and tribological behavior of pure Zn and different Zn−Ni alloy coatings [J]. Materials Chemistry and Physics, 2016, 183: 263−272. doi: 10.1016/j.matchemphys. 2016.08.026.

[7] LEE L, RÉGIS É, DESCARTES S, CHROMIK R R. Fretting wear behavior of Zn−Ni alloy coatings [J]. Wear, 2015, 330: 112−121. doi: 10.1016/j.wear.2015.02.043.

[8] GHAZIOF S, GAO W. Electrodeposition of single gamma phased Zn−Ni alloy coatings from additive-free acidic bath [J]. Applied Surface Science, 2014, 311: 635−642. doi: 10.1016/j.apsusc.2014.05. 127.

[9] SRIRAMAN K R, BRAHIMI S, SZPUNAR J A, OSBORNE J H, YUE S. Characterization of corrosion resistance of electrodeposited Zn−Ni Zn and Cd coatings [J]. Electrochimica Acta, 2013, 105: 314−323. doi: 10.1016/j.electacta.2013.05.010.

[10] FASHU S, GU C D, ZHANG J L, HUANG M L, WANG X L, TU J P. Effect of EDTA and NH_4Cl additives on electrodeposition of Zn−Ni films from choline chloride-based ionic liquid [J]. Transactions of Nonferrous Metals Society of China, 2015, 25(6): 2054−2064. doi: 10.1016/S1003-6326(15)63815-8.

[11] CONRAD H, CORBETT J, GOLDEN T D. Electrochemical deposition of γ-phase zinc−nickel alloys from alkaline solution [J]. ECS Transactions, 2011, 33(30): 85−95. doi: 10.1149/2.027201jes.

[12] EL-LATEEF H M A, EL-SAYED A R, MOHRAN H S. Role of nickel alloying on anodic dissolution behavior of zinc in 3.5% NaCl solution. Part II: Potentiodynamic, potentiostatic and galvanostatic studies [J]. Transactions of Nonferrous Metals Society of China, 2015, 25(9): 3152−3164. doi: 10.1016/S1003-6326(15)63946-2.

[13] CONDE A, ARENAS M A, de DAMBORENEA J J. Electrodeposition of Zn−Ni coatings as Cd replacement for corrosion protection of high strength steel [J]. Corrosion Science, 2011, 53(4): 1489−1497. doi: 10.1016/J.CORSCI. 2011.01.021.

[14] KIM H, POPOV B N, CHEN K S. A Novel electrodeposition process for plating Zn−Ni−Cd alloys [J]. Journal of the Electrochemical Society, 2003, 150(2): C81−88. doi: 10.1149/1.1534599.

[15] HEGDE A C, VENKATAKRISHNA K, ELIAZ N. Electrodeposition of Zn−Ni, Zn−Fe and Zn−Ni−Fe alloys [J]. Surface and Coatings Technology, 2010, 205(7): 2031−2041. doi: 10.1016/J.SURFCOAT. 2010.08.102.

[16] ELIAZ N, VENKATAKRISHNA K, HEGDE A C. Hegde, electroplating and characterization of Zn−Ni, Zn−Co and Zn−Ni−Co alloys [J]. Surface and Coatings Technology, 2010, 205(7): 1969−1978. doi: 10.1016/J.SURFCOAT. 2010.08.077.

[17] ZHENG H Y, AN M Z. Electrodeposition of Zn−Ni−Al_2O_3 nanocomposite coatings under ultrasound conditions [J]. Journal of Alloys and Compounds, 2008, 459(1−2): 548−552. doi: 10.1016/J. JALLCOM.2007.05.043.

[18] PRAVEEN B M, VENKATESHA T V. Electrodeposition and properties of Zn−Ni−CNT composite coatings [J]. Journal of Alloys and Compounds, 2009, 482(1−2): 53−57. doi: 10.1016/J.JALLCOM. 2009.04.056.

[19] FRATESI R, ROVENTI G. Corrosion resistance of Zn−Ni alloy coatings in industrial production [J]. Surface and Coatings Technology, 1996, 82(1−2): 158−164. doi: 10.1016/0257-8972(95) 02668-1.

[20] GHAZIOF S, GAO W. Zn−Ni−Al_2O_3 nano-composite coatings prepared by sol-enhanced electroplating [J]. Applied Surface Science, 2015, 351: 869−879. doi: 10.1016/j.apsusc.2015.06.010.

[21] BOSHKOV N, PETROV K, VITKOVA S. Corrosion products of zinc−manganese coatings-part. III: Double-protective action of manganese [J]. Metal Finishing, 2002, 100(6): 98−102. doi: 10.1016/ S0026-0576(02)82009-8.

[22] GANESAN S, PRABHU G, POPOV B N. Electrodeposition and characterization of Zn−Mn coatings for corrosion protection [J]. Surface and Coatings Technology, 2014, 238: 143−151. doi: 10.1016/ J.SURFCOAT.2013.10.062.

[23] BOSHKOV N, PETROV K, KOVACHEVA D, VITKOVA S, NEMSKA S. Influence of the alloying component on the protective ability of some zinc galvanic coatings [J]. Electrochimica Acta, 2005, 51(1): 77−84. doi: 10.1016/

j.electacta.2005.03.049.

[24] KAZIMIERCZAK H, HARA A, BIGOS A, OZGA P. Electrodeposition of Zn−Mn−Mo layers from citrate-based aqueous electrolytes [J]. Electrochimica Acta, 2016, 202: 110−121. doi: 10.1016/j.electacta.2016.04.005.

[25] KIMPTON H J. The production and properties of zinc−nickel and zinc−nickel−manganese electroplate [D]. Loughborough University, 2002.

[26] ABOU-KRISHA M M, ATTIA M I, ASSAF F H, EISSA A A. Influence of pH on the composition, morphology and corrosion resistance of Zn−Ni−Mn alloy films synthesized by electrodeposition [J]. International Journal of Electrochemical Science, 2015, 10: 2972−2987.

[27] EL-SEIDY A. The effect of manganese concentration on the corrosion resistance and physical properties of Zn−Ni−Mn alloy films produced by electrodeposition [J]. International Journal of Electrochemical Science, 2015, 10: 6273−6287.

[28] BODINI M E, WILLIS L A, RIECHEL T L, SAWYER D T. Electrochemical and spectroscopic studies of manganese(II), -(III), and -(IV) gluconate complexes. 1. Formulas and oxidation-reduction stoichiometry [J]. Inorganic Chemistry, 1976, 15(7): 1538−1543. doi: 10.1021/ic50161a015.

[29] WATANABE T. Nano-plating: Microstructure control theory of plated film and data base of plated film microstructure [M]. Elsevier, 2004.

[30] BIRKHOLZ M. Thin film analysis by X-ray scattering [M]. KGaA, Weinheim, FRG: Wiley-VCH Verlag GmbH & Co, 2005.

[31] FEDI B, GIGANDET M P, HIHN J Y, MIERZEJEWSKI S. Structure determination of electrodeposited zinc−nickel alloys: Thermal stability and quantification using XRD and potentiodynamic dissolution [J]. Electrochimica Acta, 2016, 215: 652−666. doi: 10.1016/j.electacta. 2016.08.141.

[32] SYLLA D, REBERE C, GADOULEAU M, SAVALL C, CREUS J, REFAIT P. Electrodeposition of Zn−Mn alloys in acidic and alkaline baths: Influence of additives on the morphological and structural properties [J]. Journal of Applied Electrochemistry, 2005, 35(11): 1133−1139. doi: 10.1007/s10800-005-9001-2.

[33] BAKER H, OKAMOTO H. ASM handbook [M]. Alloy Phase Diagrams, 1992.

[34] SYLLA D, CREUS J, SAVALL C, ROGGY O, GADOULEAU M, REFAIT P. Electrodeposition of Zn−Mn alloys on steel from acidic Zn−Mn chloride solutions [J]. Thin Solid Films, 2003, 424(2): 171−178. doi: 10.1016/S0040-6090(02)01048-9.

[35] FENG Z, REN L, ZHANG J, YANG P, AN M. Effect of additives on the corrosion mechanism of nanocrystalline zinc–nickel alloys in an alkaline bath [J]. RSC Advances, 2016, 6(91): 88469−88485. doi: 10.1039/C6RA18476F.

[36] BALLOTE LD, RAMANAUSKAS R, BARTOLO-PEREZ P. Mn oxide film as corrosion inhibitor of Zn−Mn coatings [J]. Corrosion Reviews, 2000, 18(1): 41−52. doi: 10.1515/CORRREV.2000.18.1.41.

碱性溶液中 Zn−Ni−Mn 合金涂层的电沉积与腐蚀行为

Babak ABEDINI[1], Naghi PARVINI AHMADI[1], Sasan YAZDANI[1], Luca MAGAGNIN[2]

1. Faculty of Materials Engineering, Sahand University of Technology, Tabriz, Iran;
2. Dipartimento di Chimica, Materiali e Ingegneria Chimica Giulio Natta,
Politecnico di Milano, Via Mancinelli 7, 20131, Milano, Italy

摘　要：在添加 Mn 盐的碱性溶液中进行 Zn−Ni−Mn 镀层的恒电位电沉积，研究电解液 Mn^{2+}浓度和沉积电位对涂层表面形貌、相结构和腐蚀行为的影响。腐蚀极化实验结果表明，Zn−Ni−Mn 镀层中较高的 Mn 含量可能导致形成良好的钝化层；与 Zn−Ni 涂层相比，其 R_p(极化电阻)增大 7 倍，而腐蚀电流密度显著降低。腐蚀试验后 Zn−Ni−Mn 镀层表面的 XRD 和 XPS 分析表明，钝化层由碱式氯化锌、氧化锌、碱式碳酸锌和氧化锰组成。

关键词：Zn−Ni−Mn；电沉积；碱性镀液；相结构；耐蚀性；化学成分

(Edited by Bing YANG)